Int J Adv Manuf Technol (2017) 88:1629–1637
DOI 10.1007/s00170-016-8816-9

ORIGINAL ARTICLE

Effect of plastic anisotropy of ZK60 magnesium alloy sheet on its forming characteristics during deep drawing process

Peng Lin[1] · **Ying Sun**[1] · **Chengzhong Chi**[1] · **Wenxian Wang**[1]

Received: 17 September 2015 / Accepted: 18 April 2016 / Published online: 20 May 2016

Abstract The plastic anisotropy of a ZK60 magnesium alloy sheet was investigated using uniaxial tensile tests and deep drawing tests. The earing behavior of the sheet during deep drawing was studied by both experimental and finite element analyses. The ZK60 alloy sheet exhibits higher plastic strain ratio (r) value in 45° than those in 0° and 90° to rolling direction, and the r value decreases with temperature increasing in various loading directions. A negative planar anisotropy ($\triangle r$) value results in earing in 45° to rolling direction. Higher absolute value of $\triangle r$ leads to larger average earing ratios. With drawing ratio (DR) increasing, the average earing ratio first increases to a peak and then drops, showing a bell-shape curve. The average earing ratio of cylindrical drawn cup increases as the deep drawing proceeds. At the shoulder region of drawn cups, the most reduction in thickness strain occurs in 45° to rolling direction of the sheet. At the necking region, the minimum thickness strain in 0° is lower than those in 45° and 90° directions. At the thickening region, the minimum thickness strain in 45° is lower than those in 0° and 90° directions due to the large circumferential compression stress and the large negative value of planar anisotropy $\triangle r$ value.

Keywords Plastic anisotropy · Deep drawing · Earing

✉ Peng Lin
linpeng@tyut.edu.cn

[1] Shanxi Key Laboratory of Advanced Magnesium-Based Materials, College of Materials Science and Engineering, Taiyuan University of Technology, Taiyuan 030024, People's Republic of China

1 Introduction

Magnesium (Mg) alloys have attracted a great attention in military, automotive, aerospace, and biomedical applications due to their low density, high specific strength, stiffness, biocompatibility, and reasonable cost [1, 2]. Traditionally rolled Mg alloy sheets generally have strong deformation texture and hence exhibit significant initial anisotropy during stamping forming, limiting their formability and industrial applications [3–6].

For sheets with anisotropy, ears [7] tend to form at the rim of cups during deep drawing. Consequently, the thickness distribution of drawn cups also becomes non-uniform. Generally, the occurrence of earing is undesirable since it requires an additional processing step where excess metal of the cup rim must be trimmed [7] and also demands extra load and leads to loss of production rate [8]. Therefore, understandings of the earing behavior of alloys with plastic anisotropy are vital to guide their deep drawing process.

Previous studies have demonstrated the influence of plastic anisotropy on deep drawing process. A three-dimension analysis of the cylindrical cup drawing was carried out by Doege and Seidel [9] to investigate the planar anisotropy effect, taking only a 45° section into account. Jung et al. [10] analyzed the deformation of circular and square cups by using the rigid-plastic finite-element method considering the planar anisotropy. Kishor et al. [8] developed a procedure for optimization of the initial blank to study the earing problems in cylindrical deep drawn cups with finite element method (FEM) based on the software LS-DYNA. Ohwue et al. [11] investigated the occurrence of earing for a low-carbon aluminum-killed steel and pure titanium by deep drawing tests and finite element simulation. The simulation was based on YLD89 anisotropic yield function using LS-DYNA software. However, factors influencing the ear formation and evolution such as temperature, deep drawing ratio, and deep drawing stages have not been sufficiently researched.

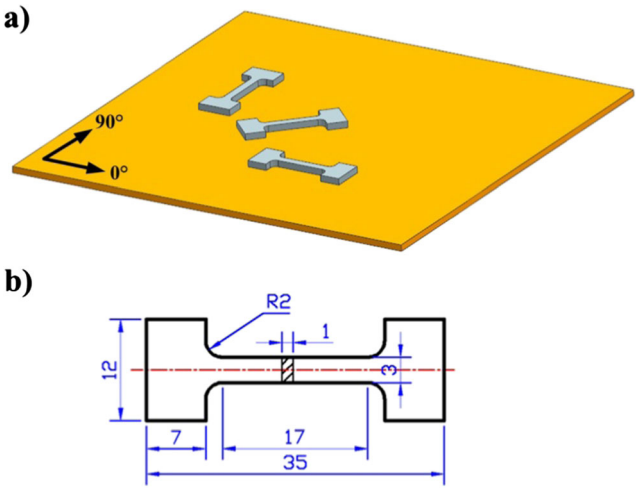

Fig. 1 **a**, **b** Geometry for uniaxial tension test (unit: mm)

In the present study, tensile tests of the ZK60 magnesium alloy sheet were carried out at elevated temperatures to characterize the mechanical anisotropy. To evaluate the anisotropy of the sheet on its forming characteristics, the cylindrical deep drawing behavior was investigated using both finite element and experimental methods and the influence of temperature and DR variables on the cylindrical deep drawing formability was also clarified.

2 Methodology

2.1 Experimental procedures

2.1.1 Material

A commercial ZK60 magnesium alloy sheet used in the present study has a chemical composition of Mg-5.78%Zn-0.76%Zr (in wt.%). The initial specimen size of the ZK60 magnesium alloy sheet was 150 × 150 × 2.3 mm (length, width, and thickness). The initial sheets were subjected to heat treatment at 325 for 60 min to obtain a homogeneous microstructure and remove residual stresses prior.

2.1.2 Uniaxial tensile test

The uniaxial tensile tests in the rolling direction (0°), transverse direction (90°), and (45°) toward to rolling direction were carried out at 200, 250, and 300 °C and strain rates of 0.1, 0.01, and 0.001 s^{-1} on a DNS200-200KN electronic universal testing machine. The specimen with the geometry is shown in Fig. 1. Each specimen was first heated to the tensile temperature at the rate of 1 °C/min and then held isothermally for 5 min to eliminate the thermal gradient before loading. The specimens were polished at the cut edges to avoid fracture at an undesired location. The permanent changes in width, thickness, and length were measured to determine the Lankford value (r value) using specimens deformed to a uniform tensile-direction strain of 0.12. Each deformation condition was repeated for three times.

2.1.3 Determination of planar anisotropy ($\triangle r$)

As mentioned above, the plastic anisotropy of sheets can be presented by plastic strain ratio (r), normal anisotropy ($\bar{r}$), and planar anisotropy ($\triangle r$), which are calculated using the following expressions [12–14]:

$$r = \frac{\varepsilon_w}{\varepsilon_t} = -\frac{\varepsilon_w}{(\varepsilon_l + \varepsilon_w)} \qquad (1)$$
$$\varepsilon_l + \varepsilon_t + \varepsilon_w = 0$$

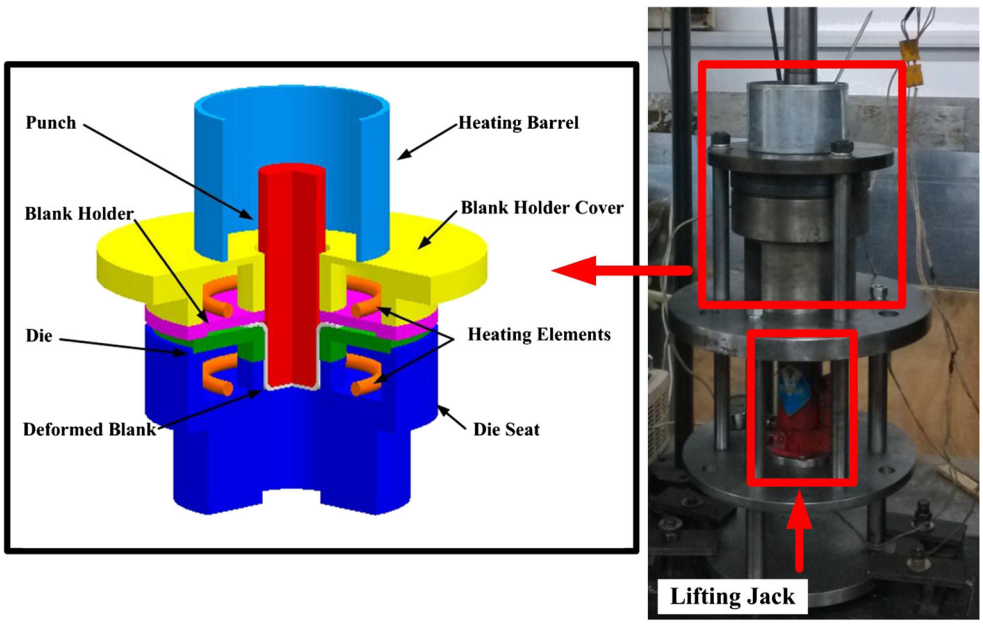

Fig. 2 Detailed view of the cylindrical deep drawing equipment and an enlarged schematic of the forming die (*left*)

Table 1 Processing parameters of cylindrical cup drawing

Punch diameter (mm)	48.4
Die diameter (mm)	55
Round radius of punch (mm)	8
Round radius of die (mm)	10
Sheet thickness (mm)	2.3
Punch speed (mm/min)	5
Gap die/blank-holder (mm)	2.76

where ε_w is the plastic strain in width direction, ε_t is the plastic strain in thickness direction, and ε_l is the strain plastic in length direction. The normal anisotropy or average plastic strain ratio was calculated by

$$\overline{r} = \frac{r_0 + 2r_{45} + r_{90}}{4} \tag{2}$$

Where r_0, r_{45}, and r_{90} denote the plastic strain ratio in 0°, 45°, and 90° to rolling direction, respectively, determined by Eq. (1). The planar anisotropy ($\triangle r$) was calculated using

$$\Delta r = \frac{r_0 + r_{90} - 2r_{45}}{2} \tag{3}$$

2.1.4 Cylindrical deep drawing test

The cylindrical deep drawing tests were carried out using the equipment on the DNS200-200KN electronic universal testing machine, as shown in Fig. 2, and the specific processing parameters are listed in Table 1. The cylindrical deep drawing experiments were conducted with a drawing ratio (DR, DR = blank diameter/punch diameter) of 1.76, 1.96, 2.17, 2.38, and 2.58 at elevated temperatures of 200, 250, and 300 °C. The blanks with various diameters were machined from the initial sheets for cylindrical cup drawing tests so as to investigate the ear height and thickness distribution. The gap between the draw die and the blank-holder was kept a constant of 2.76 mm. The temperatures of both the sheet blank and tooling were controlled by temperature controllers. Cylindrical deep drawing tests were conducted at a punch speed of 5 mm/min. Experiments were carried out with the sheet diameter of 85 to 125 mm increasingly by 10 mm. The whole blank and the contact area of the punch were coated with high-temperature grease PTFE [15] as lubricant. Additionally, the wall thickness distributions from the bottom to the flange in 0°, 45°, and 90° to rolling direction of the cylindrical drawn cups were measured using a micrometer.

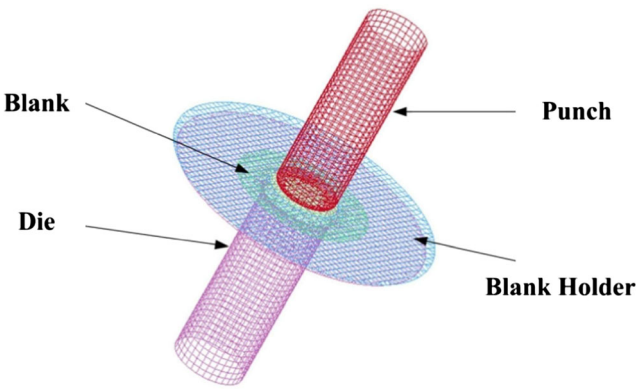

Fig. 3 Finite element model for cylindrical cup drawing

Table 2 Parameters of ZK60 magnesium sheet for numerical simulation

Parameters	Data
Density, ρ (g/cm^3)	1.8
Young's modulus, E (MPa)	44,000
Poisson's, γ	0.35
Lankford param R_0, R_{45}, R_{90}	Obtained from Table 3
Stress-strain curves	Obtained from Fig. 5
Fraction coefficient	0.2
Exponent M	8
C value	40
p value	5

2.2 FEM simulation

2.2.1 Meshing of the model

Numerical simulation was performed using the explicit finite element code LS-DYNA3D. The finite element model, as shown in Fig. 3, was established according to the dimensions used in the cylindrical deep drawing experiments. The geometry of the blank and tools was conducted by the CAD program SolidWorks 2008 SP0.0. The blanks were discreted with Belytshko-Tsay shell elements, which are in quadrilateral shape and with the minimum size of 2.0 mm, while the tools

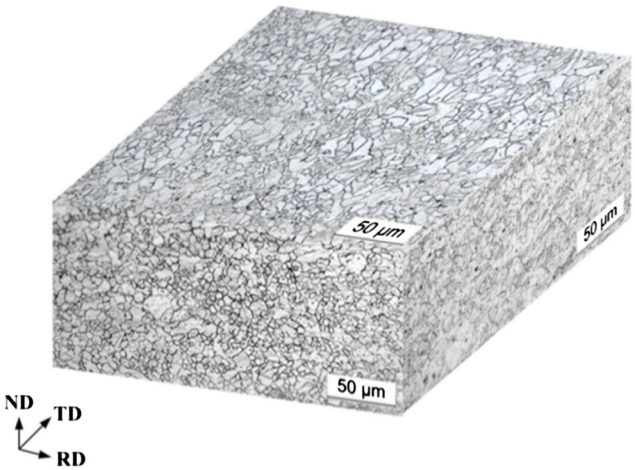

Fig. 4 The initial optical microstructure of the as-received ZK60 alloy sheet (*RD* rolling direction, *ND* normal direction, *TD* transverse direction)

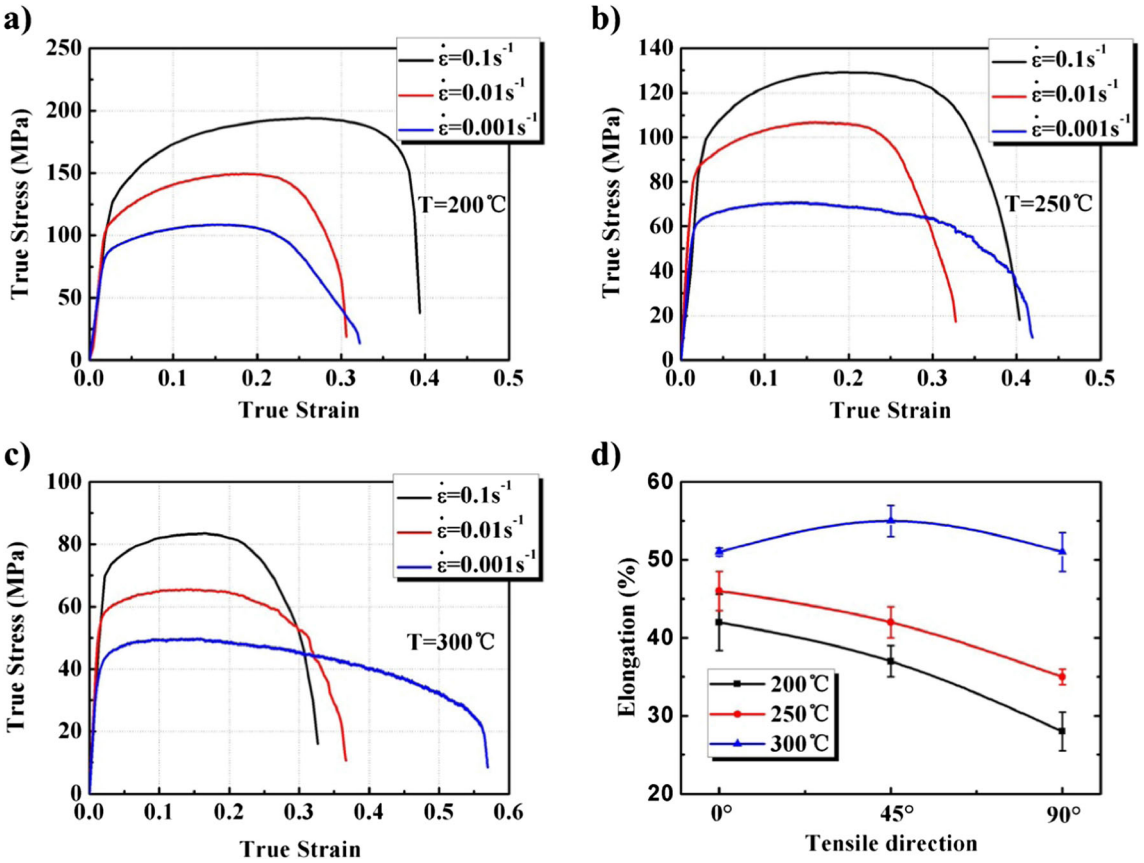

Fig. 5 Stress-strain curves of the ZK60 alloy sheet (**a**–**c**) and comparison of elongation in three tensile directions at various temperatures (**d**)

including the punch, die, and blank holder were modeled using rigid elements.

2.2.2 Constitutive model and yield criterion

The key of simulation is the selection of appropriate material model [8]. The Barlat-89 yield function [16] has been implemented in the FE code LS-DYNA3D as *MAT_3-PARAMETR_BARLAT*(MAT_036).

To include strain rate effects in the model, the yield stress was multiplied by a factor depending on the effective plastic strain rate. The Cowper-Symonds' model was used, which is described as

$$\sigma_Y\left(\varepsilon_p,\dot{\varepsilon}_p\right)=\sigma_Y^S\left(\varepsilon_p\right)\left[1+\left(\frac{\dot{\varepsilon}_p}{C}\right)^{1/p}\right] \tag{4}$$

where σ_Y^S denotes the static yield stress, C and p are material parameters, ε_p is the effective plastic strain, and ε_p is the effective plastic strain rate. Based on the material model, the strain-stress curves experimentally obtained at each temperature and strain rate of 0.001 s^{-1} (as shown in Fig. 5a–c) are employed into the software as the primary function $\sigma_Y^S(\varepsilon_p)$ for simulation. The values of C and p were obtained by nonlinear fitting. The forming limit diagram (FLD) of ZK60 alloy sheet from ref. [17] was employed into the software as a criterion for fracture prediction in the sheet-metal forming. Essential parameters for FE simulation were shown in Table 2.

3 Results and discussion

3.1 Microstructures

The initial optical microstructure of the as-received ZK60 magnesium alloy sheet is shown in Fig. 4. Obviously, the initial grain of the alloy exhibits an equiaxed morphology with average grain size of 6.3 μm. There was no fiber texture with elongated grains along rolling direction, indicating that the

Table 3 Anisotropy parameters of the ZK60 magnesium alloy sheet at various temperatures

	r			$\bar{r}$	Δr
	0°	45°	90°		
200 °C	0.973	1.170	0.988	1.075	−0.190
250 °C	0.895	1.130	0.915	1.018	−0.225
300 °C	0.824	1.060	0.836	0.945	−0.230

plastic anisotropy of the sheet is ascribed to the initial crystallographic texture.

3.2 Flow behavior and plastic anisotropy

The true stress-strain curves at various temperatures and strain rates obtained from the tensile tests are shown in Fig. 5a–c). The flow stress shows a sharp sensitivity to the deformation temperature and strain rate, that is, it increases with the temperature decreasing and strain rate increasing. The underlying mechanism was clarified in detail in ref. [18]. In addition, due to dynamic recovery, the work hardening effect of the alloy was increasingly weakened by the temperature rise and strain rate reducing. Under deformation at temperature above 250 °C and strain rate lower than 0.01 s^{-1}, no obvious work hardening is observed. Figure 5d shows the elongation to failure (ε_f) of the alloy in 0°, 45°, and 90° to rolling direction at 200, 250, and 300 °C. It is observed that ε_f in all tensile directions increased as temperature increasing, from 28 % at 200 °C to 55 % at 300 °C. ε_f has the maximum and minimum value in 0° and 90° directions, respectively, at 200 and 250 °C, while almost has the same value at 300 °C, exhibiting a decrease in the mechanical anisotropy with increasing temperature, which might be attributed to the reduction in twin generation with increasing temperature [19].

The anisotropy parameters of the ZK60 magnesium alloy sheet are shown in Table 3. The 45° samples exhibit higher r value compared with those in the other two directions, which can be explained by the high width strain during deformation [12]. The r value decreases with temperature increasing in various loading directions, which was strongly dependent on the crystal texture by rolling process [12, 20].

3.3 Cylindrical deep drawing behavior

3.3.1 Cylindrical deep drawing behavior at various temperatures

The ear height of a cylindrical deep drawn cup is dependent on the planar anisotropy of the sheet [21]. Figure 6a–c shows comparison of the experimental and simulated wall height distributions (DR = 2.17) for the drawn cup formed at 200, 250, and 300 °C, respectively. It can be observed that the drawn cup has obvious ears in 45° to rolling direction due to

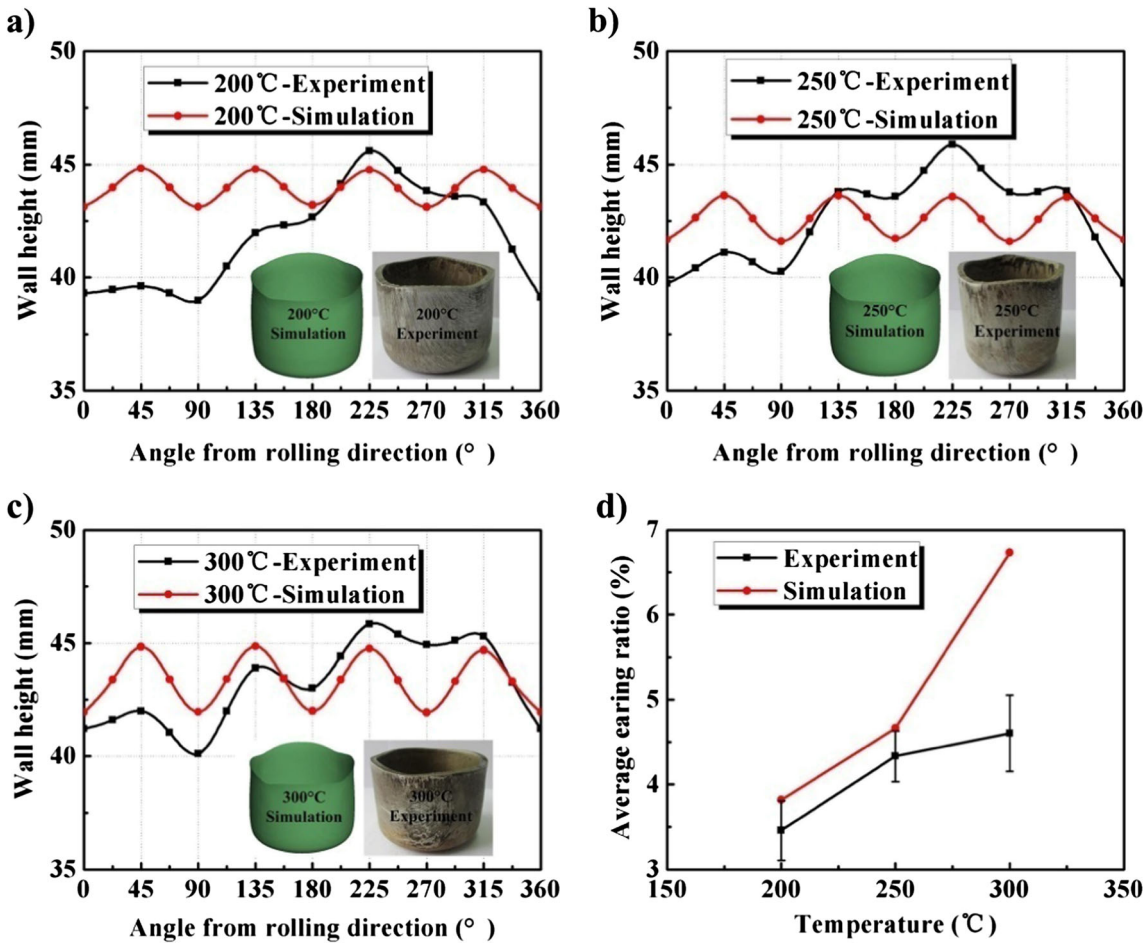

Fig. 6 Comparison of experimental and simulated wall height distribution of drawn cups with DR of 2.17 at **a** 200 °C, **b** 250 °C, and **c** 300 °C. **d** Comparison of experimental and simulated average earing ratio of drawn cups at various temperatures

the negative value of $\triangle r$, agreeing well with the FE simulation results. Figure 6d depicts the average earing ratio of the drawn cups at various temperatures, calculated by

$$Z = \left\{ \frac{\sum_{i}^{n} \left(\frac{h_{i\_\max} - h_{i\_\min}}{h_{i\_\min}} \right)}{n} \right\} \times 100\% \quad (5)$$

Where $h_{i\_\max}$ is the mean height of the cup from the bottom to the top of the ears, $h_{i\_\min}$ is the mean height of the cup from the bottom to the ear valleys, and n is the number of ears on a drawn cup. The notation (Eq. (5)) is capable of describing earing even if a local asymmetry occurs and takes ears in different orientations into account. Both experimental and simulated results show that the average earing ratio was closely dependent on the planar anisotropy $\triangle r$ value. A negative $\triangle r$

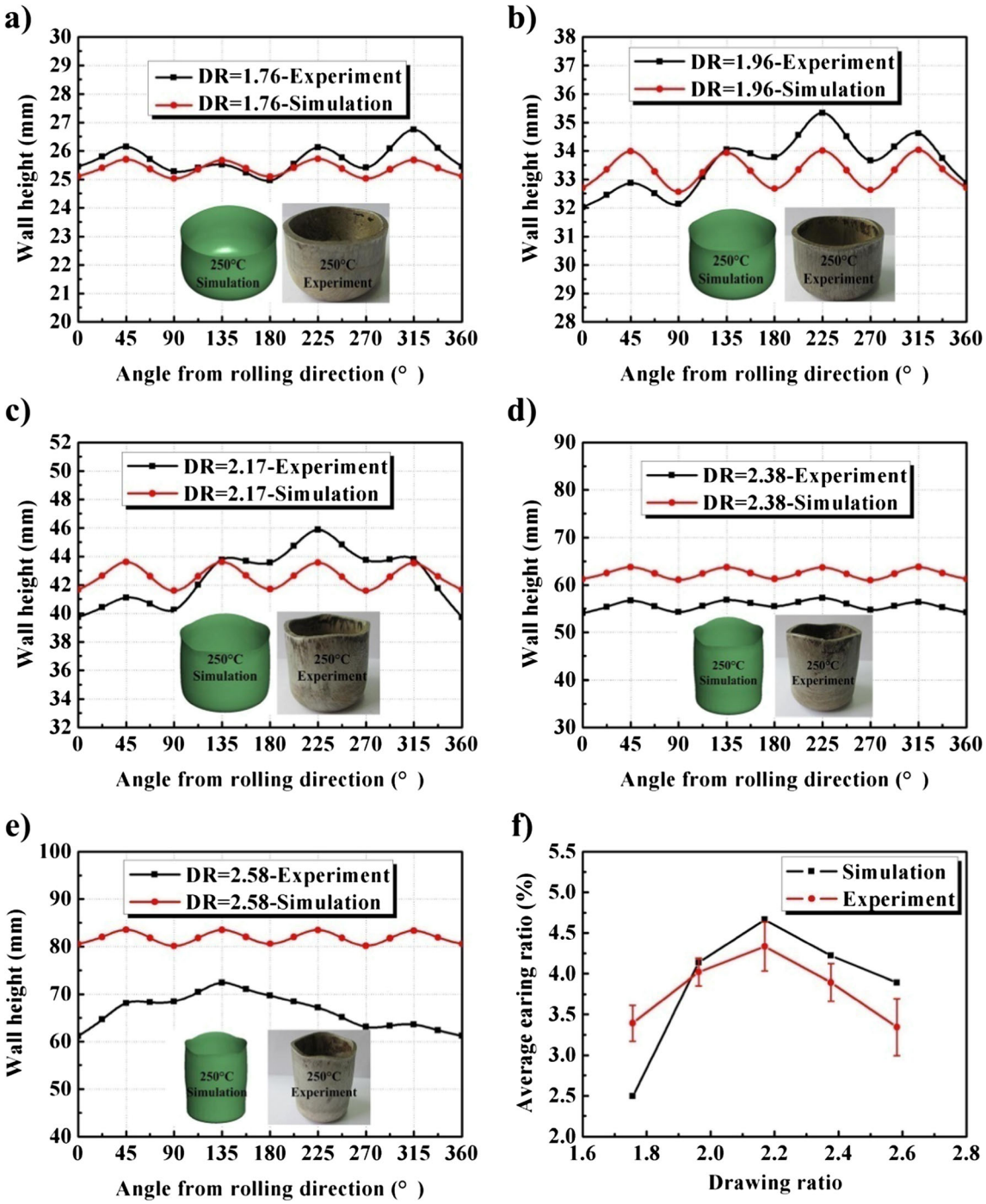

Fig. 7 Comparison of experimental and simulated wall height distribution of the drawn cups at 250 °C for various drawing ratios (**a**–**e**). Comparison of experimental and simulated average earing ratio of drawn cups at various DRs(f)

value will result in earing in 45° to rolling direction. Higher absolute value of $\triangle r$ will lead to larger average earing ratios; therefore, it increases with the forming temperature increasing.

3.3.2 Cylindrical deep drawing behavior of sheets with various DRs

Figure 7a–e shows the experimental and simulated wall height distribution of the drawn cups with various DRs at 250 °C. It is shown in Fig. 7a–c that the simulated cup wall height distribution with DR from 1.76 to 2.17 shows a good agreement with the experimental one. However, for the drawn cups with DR from 2.38 to 2.58, the simulated wall height is obviously higher than the experimental one, as shown in Fig. 7d–e. A larger value of DR represents a larger effective strain of the blank during deep drawing, which means that the deviation between simulated and experimental results is due to the increasing strain. That is because the primary function $\sigma_Y^S(\varepsilon_p)$ in the material model for simulation is based on the strain-stress curves at strain rate of 0.001 s^{-1} and the whole model only took the work hardening effect at such strain rate into account. As a result, the work hardening enhancement by strain rate increasing was ignored in the simulation, leading to a lower resistance to deformation and a higher wall height than the experimental result. Therefore, the simulation using Cowper-Symonds' model is more accurate when the effective strain is small, such as the deep drawing process with DR less than 2.17 in the present study. Figure 7f shows the average earing ratio of experimental and simulated drawn cups with various DRs at 250 °C. It shows that the DR has a large impact on the average earing ratio. The average earing ratio increases gradually to a peak and then drops with DR increasing. The maximum was obtained at the DR of 2.17. The simulated results agree well with the experimental data. This is because the average earing ratio was calculated by $h_{i\_\max}$ and $h_{i\_\min}$, both of which significantly increase with blank diameters increasing. However, the rate of $h_{i\_\min}$ increase faster than that of $h_{i\_\max}$, leading to a bell-shape curve of the average earing ratio versus DR.

3.3.3 Cylindrical deep drawing behavior in various drawing stages

Figure 8a shows the average earing ratio of experimental and simulated drawn cups with DR of 2.17 in different drawing stages at various temperatures. As seen, the average earing ratio of cylindrical drawn cups increases as the deep drawing proceeds, and in all stages, it also increases with the forming temperature increasing. The average earing ratio at 250 °C predicted by FE simulation has an approximate tendency to agree well with the experimental results at 40–80 % drawing stages. Figure 8b shows the average earing ratio of experimental and simulated drawn cups with various DRs at 250 °C in each drawing stage. It shows that the average earing ratio increases with the DR increasing at 20 and 40 % drawing stages, while increases to a peak and then drops at 60 and 80 % drawing stages. Above-mentioned results fully clarified the earing evolution during the whole drawing process.

3.4 Thickness strain distributions

The thickness strain distribution in 0°, 45°, and 90° to rolling direction of the cups drawn at 200, 250, and 300 °C is illustrated in Fig. 9a–e. There are two thinning positions (labeled with stage 1 and stage 2) and a thickening position (labeled with stage 3), located at the shoulder region, the necking region near to the punch radius and the rim of the deep-drawing cup, respectively. As the punch moves, the deformation at the shoulder region contacting the punch-nose is restricted due to the friction. However, the necking region with less work hardening has a small cross-sectional area to transmit drawing load. As a result, the main deformation is transferred from the shoulder region to the necking region. The minimum thickness strains in 0°, 45°, and 90° to rolling direction of the drawn cup as function of the deformation temperature is

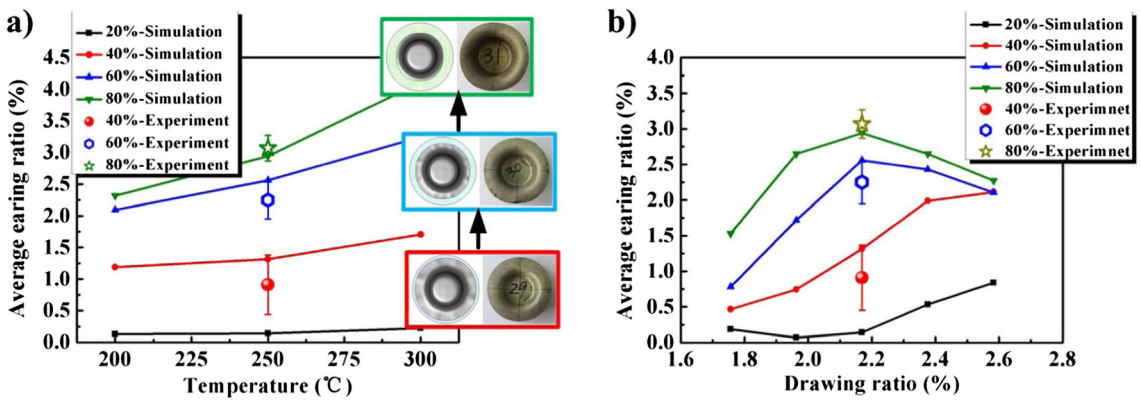

Fig. 8 **a** The average earing ratio of experimental and simulated drawn cups with DR of 2.17 in progressive drawing stages at various temperatures. **b** The average earing ratio of experimental and simulated drawn cups with various DRs at 250 °C in each drawing stage

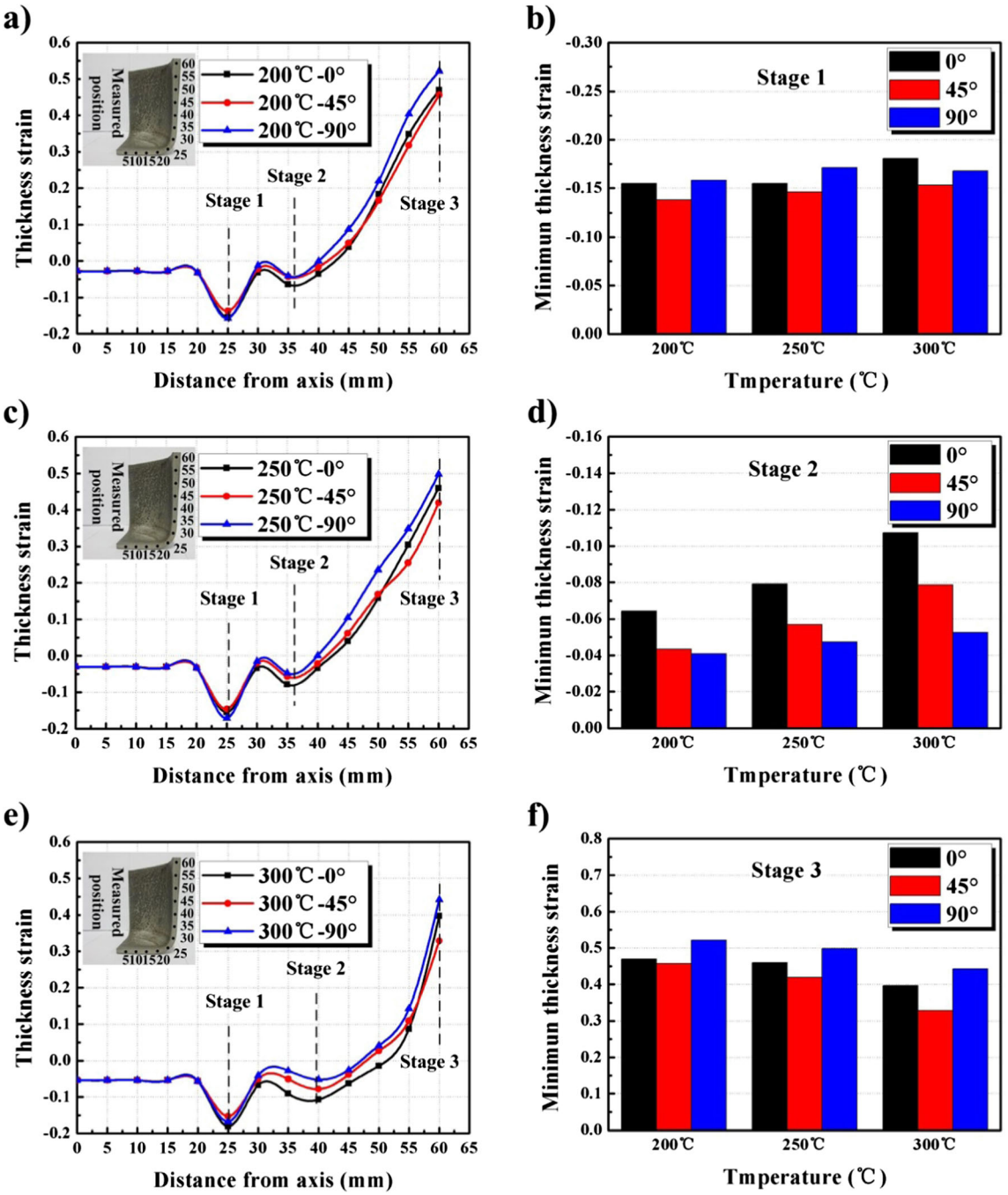

Fig. 9 Thickness strains of the drawn cup with DR of 2.17 in 0°, 45°, and 90° to rolling direction at **a** 200 °C, **c** 250 °C, and **e** 300 °C. Minimum thickness strain of the drawn cup with DR of 2.17 in 0°, 45°, and 90° to rolling direction as function of the deformation temperature: **b** stage 1, **d** stage 2, and **f** stage 3

illustrated in Fig. 9: (b) stage 1, (d) stage 2, and (f) stage 3. The minimum thickness strains (in stage 1, stage 2, and stage 3) in all the three directions increase with the deformation temperature increasing. As shown in Fig. 9b, the most reduction in the thickness strain at the shoulder region occurs in 45° to rolling direction due to the higher r value [22, 23]. In Fig. 9d, the minimum thickness strain at the necking region of the deep drawn cup in 0° is lower than those in 45° and 90° directions due to the interaction between the normal anisotropy in 0°, 45°, and 90° to rolling direction. The thickness in 0° and 90° directions is compensated and the r value in 0° direction is significantly lower than those in 45° and 90° directions. In Fig. 9f, the minimum thickness strain of the deep drawn cup in 45° is lower than those along 0° and 90° directions. As the punch moves, the edge region of the cup exists a circumferential compression stress, leading to the increase of the wall

thickness. The influence of circumferential compression stress on deep drawn cup in 0° and 90° directions is larger than that in 45° direction. Therefore, the minimum thickness strain in 45° direction is lower than those in 0° and 90° directions due to the large circumferential compression stress state and the large negative value of planar anisotropy $\triangle r$.

4 Conclusions

In this study, the influence of the plastic anisotropy on the deep drawing formability of a ZK60 alloy sheet has been investigated with experimental and simulative methods. The main conclusions are summarized as follows:

1. The ZK60 alloy sheet exhibits higher r value in 45° than those in 0° and 90° to rolling direction and the r value decreases with temperature increasing in various loading directions. The average earing ratio was closely dependent on the planar anisotropy $\triangle r$ value. A negative $\triangle r$ value results in earing in 45° to rolling direction. Higher absolute value of $\triangle r$ leads to larger average earing ratios.
2. With DR increasing, the average earing ratio first increases to a peak and then drops, showing a bell-shape curve. The deviation between simulated and experimental cup wall height value will be enlarged with DR increasing due to the use of Cowper-Symonds' model for simulation, which ignored the work hardening enhancement by strain rate increasing. The average earing ratio of cylindrical drawn cup increases as the deep drawing proceeds.
3. At the shoulder region of drawn cups, the most reduction in thickness strain occurs in 45° to rolling direction of the sheet. At the necking region, the minimum thickness strain in 0° is lower than those in 45° and 90° to rolling direction. At the thickening region, the minimum thickness strain in 45° is lower than those in 0° and 90° directions due to the large circumferential compression stress state and the large negative value of planar anisotropy $\triangle r$ value.

Acknowledgments This project was supported by the National Natural Science Foundation of China (Grant No. 51505323, 51375328, and 51175363)

References

1. Li QZ, Tian B (2012) Mechanical properties and microstructure of pure polycrystalline magnesium rolled by different routes. Mater Lett 67:81–83
2. Kulekci MK (2008) Magnesium and its alloys applications in automotive industry. Int J Adv Manuf Technol 39:851–865
3. Agnew SR, Duygulu Ö (2005) Plastic anisotropy and the role of non-basal slip in magnesium alloy AZ31B. Int J Plast 21:1161–1193
4. Kleiner S, Uggowitzer PJ (2004) Mechanical anisotropy of extruded Mg-6% Al-1% Zn alloy. Mater Sci Eng A 379:258–263
5. Song B, Xin RL, Guo N, Xu JB, Sun LY, Liu Q (2015) Dependence of tensile and compressive deformation behavior on aging precipitation in rolled ZK60 alloys. Mater Sci Eng A 639:724–731
6. Chan LC, Lu XZ (2014) Material sensitivity and formability prediction of warm-forming magnesium alloy sheets with experimental verification. Int J Adv Manuf Technol 71:253–262
7. Yan H, Chen RS, Han EH (2010) Room-temperature ductility and anisotropy of two rolled Mg-Zn-Gd alloys. Mater Sci Eng A 527:3317–3322
8. Saxena RK, Dixit PM (2009) Finite element simulation of earing defect in deep drawing. Int J Adv Manuf Technol 45:219–233
9. Kishor N, Ravi Kumar D (2002) Optimization of initial blank shape to minimize earing in deep drawing using finite element method. J Mater Process Technol 130–131:20–30
10. Doege E, Seidel M (1988) Influence of anisotropy in sheet metal forming. Model Metal Form Process 123–130
11. Jung DW, Song IS, Yang DY (1995) An improved method for the application of blank-holding force considering the sheet thickness in the deep-drawing simulation of planar anisotropic sheet. J Mater Process Technol 52:472–488
12. Ohwue T, Kobayashi Y (2014) Analysis of earing in circular-shell deep-drawing of bcc and hcp sheet metals. Procedia Eng 81:887–892
13. Yi S, Bohelen J, Heinemann F, Letzig D (2010) Mechanical anisotropy and deep drawing behavior of AZ31 and ZE10 magnesium alloy sheets. Acta Mater 58:592–605
14. Keeler SP (1968) Understanding sheet metal formability. National Steel Corporation, USA
15. Leu D-K (1997) Prediction of the limiting drawing ratio and the maximum drawing load in the cup drawing. Int J Mach Tools Manuf 37(2):201–213
16. Zhang SH, Zhang K, Xu YC, Wang ZT, Xu Y, Wang ZG (2007) Deep-drawing of magnesium alloy sheets at warm temperatures. J Mater Process Technol 185:147–151
17. Barlat F, Lian J (1989) Plastic behavior and stretch ability of sheet metals. Part I. A yield function for orthotropic sheets under plane stress conditions. Int J Plast 5:51–66
18. Liu HW, Yao SJ, Liu WL (2007) Forming limit diagram of magnesium alloy ZK60 at elevated temperature. Adv Mater Res 308–310:2442–2445
19. Lin P, He ZB, Yuan SJ, Shen J (2012) Tensile deformation behavior of Ti-22Al-25Nb alloy at elevated temperatures. Mater Sci Eng A 556(11):617–624
20. Chino Y, Kimura K, Hakamada M, Mabuchi M (2008) Mechanical anisotropy due to twinning in an extruded AZ31 Mg alloy. Mater Sci Eng A 485:311–317
21. Gall S, Coelho RS, Müller S, Reimers W (2013) Mechanical properties and forming behavior of extruded AZ31 and ME21 magnesium alloy sheets. Mater Sci Eng A 579:180–187
22. Hosford WF, Caddell RM (2007) Metal forming: metallurgy and mechanics. Cambridge University Press, Cambridge
23. Shimizu T, Ogawa M, Yang M, Manabe K (2014) Plastic anisotropy of ultra-thin rolled phosphor bronze foils and its thickness strain evolution in micro-deep drawing. Mater Des 56:604–612